Available online at www.sciencedirect.com
SCIENCE DIRECT®
Acta Materialia 53 (2005) 2595–2605
Acta MATERIALIA
www.actamat-journals.com

Fatigue threshold *R*-curves for predicting reliability of ceramics under cyclic loading

J.J. Kruzic [a,*], R.M. Cannon [b], J.W. Ager III [b], R.O. Ritchie [b,c]

[a] *Department of Mechanical Engineering, Oregon State University, 204 Rogers Hall, Corvallis, OR 97331, USA*
[b] *Materials Sciences Division, Lawrence Berkeley National Laboratory, Berkeley, CA 94720, USA*
[c] *Department of Materials Science and Engineering, University of California, Berkeley, CA 94720, USA*

Received 7 December 2004; received in revised form 7 December 2004; accepted 8 February 2005
Available online 2 April 2005

Abstract

For monolithic, grain-bridging ceramics, the crack-size dependence of the fatigue threshold during bridging zone development presents a difficulty in its application in design. This paper demonstrates how a fatigue threshold *R*-curve may express this crack-size dependence, analogous to the traditional fracture toughness *R*-curve, and may be used to predict the endurance limit and retained strength under cyclic loading conditions. Furthermore, the fatigue threshold *R*-curve may be deduced from the behavior of millimeter-scale, through-thickness, fatigue cracks via an accurately measured crack bridging stress profile. Both an alumina ceramic with large steady-state bridging zones (~2 mm), where the predicted and experimentally measured fatigue threshold *R*-curves agree well over a range of crack sizes from 0.06 to 7 mm, and a (Y_2O_3-MgO)-doped Si_3N_4 ceramic, where bridging zones are much shorter (~100 μm), are investigated. The approach provides a useful alternative to performing difficult short-crack fatigue experiments, particularly for materials with small bridging zones.
© 2005 Acta Materialia Inc. Published by Elsevier Ltd. All rights reserved.

Keywords: Ceramics; Mechanical properties (fatigue, *R*-curves, crack bridging)

1. Introduction

While grain bridging has proved to be a potent mechanism for creating tough ceramics [1–9], under cyclic loads these materials are typically susceptible to premature failure by subcritical crack propagation owing to degradation of the bridges [9–18]. Moreover, as bridging only develops with crack extension, there is an inherent effect of crack size on the material toughness [1–5] and, as well, on the cyclic fatigue-crack growth resistance [11] for cracks shorter than the steady-state bridging-zone lengths. Such crack-size effects on fracture toughness are expressed in the form of a resistance- or *R*-curve, which allows for failure predictions based on the loading conditions and initial flaw size [19]. For bridging ceramics, methods have been developed for predicting such *R*-curves based on measured bridging stress functions for cracks with steady-state bridging zones [2,20–22]. However, such methods are non-conservative for predicting reliability under cyclic loading conditions owing to damage in the bridging zone; and there is currently no analogous methodology for use with fatigue. Furthermore, as bridging is achieved with weak grain boundaries that permit intergranular fracture, the absolute threshold for initial crack extension is reduced versus that for nonbridging materials and is far too conservative for an alternative design criterion.

Accordingly, the goal of the present paper is to develop a framework for the prediction of reliability in bridging ceramics under cyclic loading conditions based on a fatigue threshold *R*-curve [23–25], which gives the threshold as a function of crack extension. The

* Corresponding author. Tel.: +1 541 737 7027; fax: +1 541 737 2600.
E-mail address: kruzicj@engr.orst.edu (J.J. Kruzic).

1359-6454/$30.00 © 2005 Acta Materialia Inc. Published by Elsevier Ltd. All rights reserved.
doi:10.1016/j.actamat.2005.02.018

proposed method is analogous to the traditional fracture toughness R-curve approach, and is achieved using measured bridging stress distributions.

2. Background

One consequence of making high-toughness ceramics has been that such materials become susceptible to fatigue failure due to progressive degradation of the toughening under cyclic loading. This is in contrast to untoughened ceramics which are essentially immune to cyclic fatigue, within the proviso that they may experience environmentally assisted sub-critical growth during cyclic loading. Fatigue-crack growth rates in ceramics at a specific load ratio ($R = K_{min}/K_{max}$) tend to follow a classical Paris power–law relationship:

$$\frac{da}{dN} = A(\Delta K)^m, \tag{1}$$

where A and m are scaling constants, da/dN is the growth rate, ΔK is the stress-intensity range ($K_{max} - K_{min}$), and K_{max} and K_{min} are, respectively, the maximum and minimum values applied during a loading cycle. The Paris law exponent is typically very large for ceramics, i.e., $m \sim 15$–100; consequently, propagating fatigue cracks quickly grow to failure unless they are in a decaying ΔK situation. Because of this, the fatigue threshold, ΔK_{TH}, below which cracks are presumed not to propagate under cyclic loads is often considered as a critical parameter in the fatigue of ceramics.[1]

In light of this, the precise definition of the fatigue threshold is a central issue. The majority of fatigue-crack growth tests performed to date on ceramic materials have used millimeter-scale (so called "large") cracks growing in standard fracture mechanics specimens [9,12–16,29–31]. These experiments typically are believed to represent the behavior of cracks with steady-state bridging zones, where bridges are created and destroyed at a roughly equal rate and the zone size is equilibrated at each K value. Crack-size effects on the fatigue threshold are thus ignored in such experiments, and the measured fatigue thresholds are non-conservative when compared to those from smaller cracks with developing, or transient, bridging zones [11]. Since relevant crack sizes in ceramics for structural use will likely be several orders of magnitude smaller than those in such test specimens, effects of crack size must be addressed if the fatigue threshold is to be used as a design parameter.

One approach to assessing the effects of developing, or transient, bridging zones on the fatigue threshold is to conduct direct experiments on functionally small or short cracks. In the context of this paper, cracks are considered short or small if comparable in size to, or less than, one of three characteristic dimensions, namely, the microstructure (microstructurally-small), the extent of local inelasticity ahead of a crack tip (mechanically-short/small), and/or the extent of the zone causing crack-tip shielding or bridging behind a crack tip (functionally-short/small) [32,33]. Short cracks meet such conditions in only one dimension, i.e., the crack length, and small cracks meet one or more such conditions in both dimensions. A functionally-short crack has limited crack-tip shielding, yet samples the microstructure statistically because of its extensive crack front [34]. Conversely, functionally-small cracks are small in all dimensions, as typified by a small, semi-elliptical surface flaw. When small cracks are comparable in size to microstructural entities, in addition to reduced shielding, biased sampling of microstructurally weak paths may occur. Due to these restrictions in shielding and microstructural sampling, the crack-growth resistances of microstructurally small cracks generally tend to be more variable but at the extreme are among the lowest. In addition, residual stresses either from contact damage or from thermal expansion mismatch may act more strongly on small cracks; if unappreciated or unaccounted, they lower the effective or operational R-curve for small cracks [35–37]. While direct short or small crack testing seems attractive, there are many experimental difficulties in creating, propagating, and monitoring very small fatigue cracks in ceramics. Indeed, for materials with steeply rising R-curves, most attempts at such experiments have found that the practical crack sizes for testing were too long compared to the bridging-zone length to notice any small-crack effects [27,38–40].

Recently, we have proposed an alternative approach [11] which first involves determining the steady-state contribution of bridging, $K_{SS,br}$, in reducing the applied stress intensity; superposition is then used to subtract this bridging stress intensity from the measured steady-state threshold, $K^{TH}_{SS,max}$, to obtain an intrinsic threshold for the tip of an unbridged crack, $K^{TH}_{o,max}$, using [11]:

$$K^{TH}_{o,max} = K^{TH}_{SS,max} - K_{SS,br}. \tag{2}$$

In ceramics the threshold depends more strongly on the value of the maximum stress intensity, K_{max}, as opposed to the stress-intensity range, ΔK, per se [9,12–14,41]; consequently, fatigue thresholds are expressed here in terms of K^{TH}_{max}, noting that this may easily be related to ΔK through the load ratio, $R = K_{min}/K_{max}$. Also, since there is no cyclic fatigue effect in the absence of bridging for the most brittle ceramics, $K^{TH}_{o,max}$ may be thought of as the intrinsic toughness of the material, K_o, viz.:

$$K^{TH}_{o,max} = K_o. \tag{3}$$

[1] Alternatively, the fatigue threshold can be described in terms of the maximum stress intensity, K^{TH}_{max}, as Eq. (1) can be rewritten as $da/dN = A'(\Delta K)^p(K_{max})^n$ where $A' = A(1 - R)^n$ and $(n + p) = m$ [26,27]. With brittle materials such as ceramics, $n \gg p$ [28].

This approach gives a worst-case fatigue threshold, K_o for a bridging material below which cracks of all sizes should not propagate, provided they are large enough to statistically sample the "continuum" microstructure. A disadvantage of designing with this method, however, is that it is too conservative. In reality most short/small cracks will arrest after a short amount of subcritical growth due to the increased bridging [11]; accordingly a methodology is needed that predicts the conditions under which short/small fatigue cracks will arrest versus grow to failure. In order to address these problems, in the present work we propose the use of a fatigue threshold *R*-curve and demonstrate how this may be derived from traditional long-crack fatigue experiments by determining the bridging stresses for near-threshold steady-state fatigue cracks.

3. Procedures

3.1. Materials

A commercial 99.5% pure alumina (AD995, Coors Technical Ceramics Co., Oak Ridge, TN) was chosen as a model material due to the fact that it exhibits large steady-state bridging zones (~2 mm) near the fatigue threshold [11]. This permitted direct measurements of fatigue thresholds over a range of crack sizes that were under transient conditions, i.e., where the bridging zone was still being developed. Such experiments provided data for the fatigue threshold *R*-curve which was then compared with predictions derived from a deduced bridging stress distribution. The alumina had a wide grain size distribution, with a nominal, average size of ~25 μm; more complete information on the material may be found in Ref. [11]. Additionally, a gas pressure sintered, self-reinforced Si_3N_4 (with 5 wt% Y_2O_3 and 2 wt% MgO, added, designated YM-Si_3N_4) ceramic was used to demonstrate methods for predicting the fatigue threshold *R*-curve in a material with small bridging zones (~100 μm) where short/small crack testing is prohibitively difficult. The reinforcing grains had a mean diameter of 0.28 μm with an aspect ratio of ~7; details on the processing and microstructure of this material can be found elsewhere [42–44].

3.2. Fatigue threshold experiments

Fatigue-crack growth experiments were conducted on standard compact-tension, C(T), specimens (width, $W \approx 17$ and 19 mm for the Al_2O_3 and Si_3N_4, respectively; thickness, $B \approx 3$–3.5 mm) in general accordance with ASTM standard E647. Complete details of the fatigue-crack growth procedures are in Ref. [11]; a brief summary of issues pertinent to the measurement of fatigue thresholds is presented here. Fatigue cracks were initiated from straight machined notches (length $a_o \approx 4$–5 mm) under cyclic loading conditions (25 Hz sine wave, load ratio, $R = 0.1$), after which the cracks were grown to a specified length, as monitored using back-face strain compliance methods [45]. Notch root radii, ρ, ranged from ~15 to 150 μm, with the sharpest notches used for the smallest crack sizes. In all cases, data collection did not begin until the amount of fatigue-crack extension from the notch, Δa_f, exceeded ρ, at which point the influence of the notch field on the stress intensity could be considered to be negligible [46,47]. In order to measure the fatigue threshold, the applied stress-intensity range was reduced at a roughly constant ΔK-gradient ($=[d\Delta K/da]/\Delta K$) of -0.08 mm^{-1}. Based on previous results [11], this ΔK-gradient was low enough in AD995 alumina to achieve steady-state bridging zones for cracks with $\Delta a_f > 2$ mm in the range of growth rates from $\sim 10^{-8}$ to 10^{-10} m/cycle. Using three methods, the fatigue threshold was measured as a function of crack extension for Δa_f ranging from 60 μm to 6.5 mm, with the threshold operationally defined as the lowest stress intensity at which the fatigue-crack growth rate could be measured and does not ever exceed $\sim 10^{-10}$ m/cycle. For the Si_3N_4, which has more than an order of magnitude smaller bridging zone (~100 μm), only the steady-state (i.e., long-crack) fatigue threshold was obtained.

3.3. Quantification of bridging stresses in AD995-Al_2O_3

As the bridging stress distribution, $\sigma_{br}(x)$, for a near-threshold steady-state fatigue crack in AD995 alumina was determined in a previous study [11], the methods are only outlined here. First, a fatigue crack was grown for ~3 mm, i.e., through the entire bridging-zone length, near the fatigue threshold ($da/dN < 7 \times 10^{-10}$ m/cycle). The length of the bridging zone, *L*, was measured using multi-cutting compliance methods [11,48], whereby the crack wake was incrementally cut out using a diamond saw while making compliance measurements after each incremental cut. By noting the notch length where the compliance began to increase, a roughly $L = 2$ mm bridging-zone length was determined for close to the threshold. Additionally, the shape of the bridging stress distribution, normalized by the maximum bridging stress, σ_{max}, was determined using [48]:

$$\frac{\sigma_{br}(x)}{\sigma_{max}} = \frac{C^2(a)C'_u(x)}{C'(a)C_u^2(x)}, \tag{4}$$

where $C(a)$ is the traction-free compliance (i.e., that of the same length crack, determined optically, but neglecting bridges), $C_u(x)$ is the observed compliance after cutting to the position x measured from the load-line, and $C'(z) = dC(z)/dz$.

In order to deduce the value of σ_{max}, crack-opening displacements, $u_{tot}(x)$, were measured in a field-emission scanning electron microscope (FESEM) with the sample loaded to $K = 3.0$ MPa $\sqrt{m}$, which was 6% lower[2] than the lowest measured steady-state fatigue threshold, $K^{TH}_{SS,max}$. The crack-opening displacements and bridging stress distribution are related through the double integral equation [22],

$$-\frac{1}{E'}\int_0^a \int_{\max(x,x')}^a h(a',x)h(a',x')\sigma_{br}(x')\,da'\,dx' = u_{tot} - u_{app}, \tag{5}$$

where E' is the elastic modulus (E in plane stress, $E/(1-\nu^2)$ in plane strain, where ν is Poisson's ratio) while the weight function, h, is geometry specific and may be found for the C(T) specimen in Ref. [49]. Also used in Eq. (5) are the displacements due to the applied loading, u_{app}, for an unbridged crack at a given applied stress intensity, K_{app}, which may be calculated as [50]:

$$u_{app} = \frac{1}{E'}\int_x^a K_{app}(a')h(a',x)\,da'. \tag{6}$$

Combining the normalized bridging stress distribution from Eq. (4) with Eqs. (5), (6) allows a value for σ_{max} to be obtained; this was chosen to be the stress which gave a crack-opening profile nearest that measured experimentally, as determined by the least-squares method.

3.4. Quantification of bridging stresses in YM-Si_3N_4

Due to the small bridging zones in YM-Si_3N_4, the multi-cutting technique described above was not considered applicable for bridging stress determination. Micro-Raman spectroscopy has been used previously to evaluate stresses in Si_3N_4 by measuring shifts in the 862 cm^{-1} peak [51] and, more specifically, to measure bridging stress distributions behind crack tips [52–54]. Here we adopted this methodology to measure bridging stresses for a C(T) fatigue sample last tested near-threshold and re-loaded in situ to ~95% of the measured fatigue threshold, $K^{TH}_{SS,max}$. Specifically, a 488 nm laser was focused using an optical microscope with a 50× objective to a ~1 μm spot size on the sample surface. Laser power at the surface was kept below 5 mW to avoid effects due to sample heating. Scattered light was directed through a holographic laser line filter and into a 640 mm single spectrometer where 200 s exposures were collected using a liquid nitrogen cooled, back-thinned CCD camera. Bridging stresses were measured along the crack wake at 6 μm increments moving away from the crack tip until the shift in the Raman peak, and thus the corresponding bridging stresses, were essentially zero (~100 μm). Effects due to ambient temperature variations and/or instrument drift were avoided by recalibrating after every 3–5 bridging stress measurements using an internal zero stress reference (a part of the sample far away from the crack). The zero stress peak position corresponding to each bridging stress measurement was determined by linear interpolation between the appropriate calibration points.

Because the stress dependence of the Raman shift of the 862 cm^{-1} peak for Si_3N_4 can be affected by changes in chemical composition [52], particularly in the presence of SiAlON structures, a calibration was performed for our sample composition using a 2 mm by 3 mm cross-section beam in four-point bending at a peak stress of ±400 MPa. The laser was moved in 150 μm increments along the bend beam to record the peak shift with changing stress, again using an internal zero stress reference, as described above, which was recalibrated every 3–5 measurements. This calibration gave an average piezo-spectroscopic coefficient, Π_{avg}, of -1.77 ± 0.23 cm^{-1}/GPa. This value falls between those obtained by Pezzotti et al. [52,53] for high purity Si_3N_4 (-2.22 cm^{-1}/GPa) and for Si_3N_4 materials sintered with Al_2O_3 which contain SiAlON phases (-1.63 to -1.69 cm^{-1}/GPa).

3.5. Fatigue threshold R-curve predictions

The methods used in the present study to predict fatigue thresholds as a function of crack length, i.e., a fatigue threshold R-curve, are based on those used to predict classical fracture toughness R-curves [2,20–22]. Specifically, the toughening contribution of bridging, K_{br}, is deduced by integrating the steady-state bridging stress distribution, in this case using the weight function approach [55]:

$$K_{br} = \int_0^a h(x,a)\sigma_{br}(x)\,dx. \tag{7}$$

For $\Delta a > L$, integrating Eq. (7) gives the steady-state bridging contribution, $K_{SS,br}$, which pertains at K_{max} and is insensitive to crack length, while for $\Delta a < L$ the transient bridging contributions that exist during the development of the bridging zone are determined. In the present case, σ_{br} represents the (nearly) fully degraded bridging stress distribution for a crack loaded almost at K_{max} while near the steady-state fatigue threshold, and accordingly through the use of Eq. (7), the near-threshold bridging contributions for any crack length may be deduced, allowing the prediction of a fatigue threshold R-curve via:

$$K^{TH}_{max}(a) = K_o + K_{br}(a), \tag{8}$$

[2] Note that in the present study, additional fatigue thresholds were measured beyond those in Ref. [11]. Accordingly, there are slight variations in the values used in the present work compared to that study.

where K_o may be determined from Eqs. (2), (3), i.e., from the measured steady-state threshold and the computed $K_{SS,br}$.

4. Results

4.1. Fatigue threshold results

Results showing typical fatigue-crack growth rate behavior for AD995 alumina, in the form of $da/dN - \Delta K$ curves for a range of different crack sizes, are plotted in Fig. 1(a); Fig. 1(b) shows the corresponding steady-state fatigue-crack growth results for the YM-Si_3N_4. From Fig. 1(a) it is apparent that there is a distinct crack-size effect on the fatigue threshold; indeed, ΔK_{TH} values were roughly 50% lower for functionally-short cracks where $\Delta a_f = 60$ μm when compared to steady-state cracks with $\Delta a_f > L = 2$ mm. Because typical fatigue thresholds are measured on nominally steady-state cracks which are generally many millimeters in length, Fig. 1(a) illustrates the necessity of considering the fatigue properties for realistic flaw sizes in ceramics, i.e., in the tens to hundreds of micrometers.

One approach to this problem is the use of a fatigue threshold R-curve, shown in Fig. 2 in terms of K_{max}^{TH} for AD995 alumina. The data points in Fig. 2 represent measured fatigue thresholds plotted as a function of the fatigue crack extension, Δa_f, from the starter notch when the threshold was measured. For crack sizes where $\Delta a_f > L$, these fatigue thresholds correspond to steady-state fatigue cracks, where bridges are created and exhausted at roughly equal rates and the nature of the bridging zone uniquely corresponds to the applied ΔK level. Such steady-state fatigue thresholds should not be history- or size-dependent, meaning that steady-state conditions are always maintained while approaching the fatigue threshold (a condition more often assumed than proven [11]). For transient cracks ($\Delta a_f < L$ at the specified K level or velocity), the measured fatigue thresholds are certainly size-dependent; however, it is presumed for most samples that any history dependence on the short-crack thresholds should be minimal for cracks grown

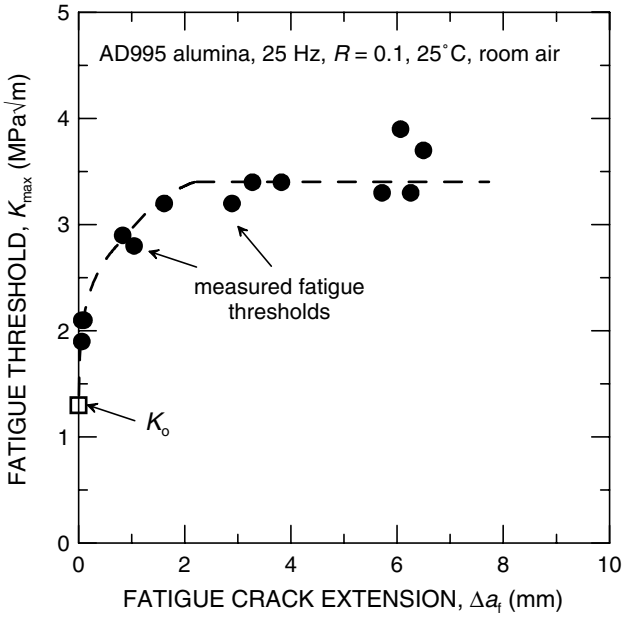

Fig. 2. Measured fatigue thresholds in AD995 alumina expressed in terms of K_{max} as a function of the crack size when the threshold was achieved.

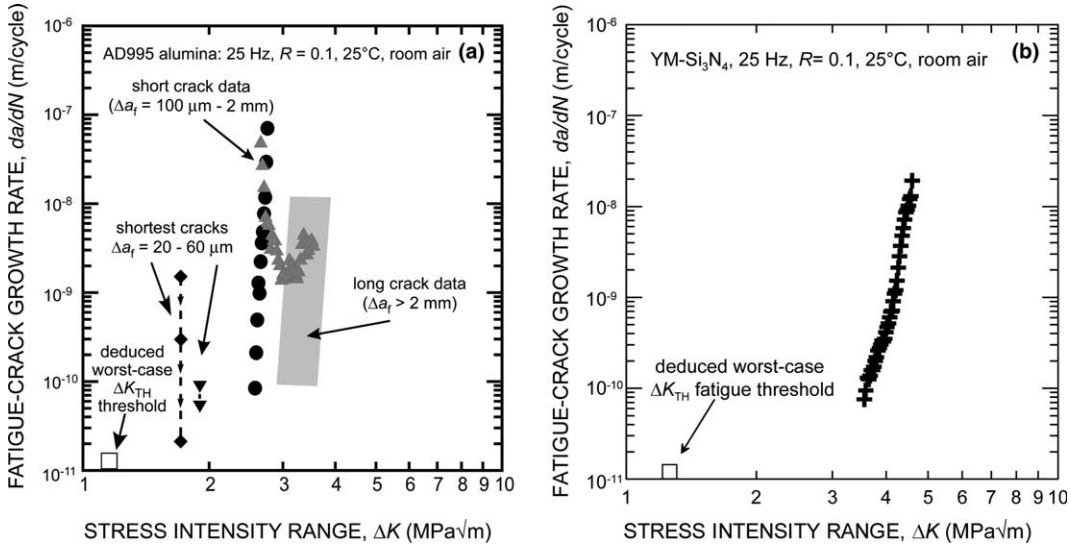

Fig. 1. Fatigue-crack growth rate data for (a) AD995 alumina and (b) YM-Si_3N_4. (a) Results for a range of crack sizes are shown during the development of the bridging zone, illustrating the need to understand fatigue thresholds at relevant crack sizes. (b) Due to the much smaller bridging zone in the Si_3N_4 material (~100 μm), similar short crack tests were not possible.

under identical conditions to the steady-state cracks, where no history dependence was observed for growth rates in the 10^{-10}–10^{-8} m/cycle range [11]. In some cases, however, initial growth rates were higher than 10^{-8} m/cycle and the measured threshold may have been elevated by history effects if bridges that formed at the higher growth rates had not been degraded sufficiently at the measured fatigue threshold. A reasonably conservative assessment of the data would be to use a lower-bound estimate for the range of available fatigue threshold data at each crack size, noting that a significant, unaccounted scatter exists in the crack-growth data, possibly owing to inherently stochastic growth through the microstructure.

4.2. Fatigue threshold R-curve predictions

Fig. 3(a),(b) shows the bridging stress distributions for a near-threshold steady-state fatigue crack in AD995 alumina, deduced using Eqs. (4)–(6), and in YM-Si_3N_4, determined using Raman spectroscopy, respectively. Since the cracks were grown near the fatigue threshold ($da/dN < 7 \times 10^{-10}$ m/cycle) through the entire bridging zone, these are considered to be reasonable estimates of the fully degraded bridging stress distributions for threshold fatigue cracks reloaded just below the level necessary to cause crack extension. Indeed, for AD995 alumina, the lowest measured steady-state threshold was $K_{max}^{TH} = 3.2$ MPa $\sqrt{m}$, while for the single Si_3N_4 sample, the threshold was $K_{max}^{TH} = 3.9$ MPa $\sqrt{m}$; both were loaded to 0.2 MPa $\sqrt{m}$ below those values. For the former case, the lowest measured threshold is used as the basis for the fatigue threshold *R*-curve predictions in order to be conservative. To get accurate estimates in both cases, 0.2 MPa $\sqrt{m}$ must be split between, and added to, the deduced steady-state bridging contribution, $K_{SS,br}$, and the intrinsic crack-tip fracture resistance, K_o, values. Two common ways in which this has been done are: (i) to add the additional stress intensity proportionately to $K_{SS,br}$ and K_o or (ii) to assume that the bridging is saturated and so add the entirety to K_o [11,22]. Since the first method gives more conservative estimates for $\Delta K_{o,TH}$ and the initial part of the fatigue threshold *R*-curve, it is used in the present analysis.

The entire bridging stress distributions was integrated using Eq. (7), after which 0.1 MPa $\sqrt{m}$ was added back as described above; the resulting assessment of the steady-state bridging contribution yielded values of $K_{SS,br}$ of 1.9 MPa $\sqrt{m}$ for AD995 alumina and 2.5 MPa $\sqrt{m}$ for the YM-Si_3N_4. Worst-case, intrinsic fatigue thresholds were then assessed according to Eq. (2), giving values of $K_o = 1.3$ MPa $\sqrt{m}$ for AD995 alumina and $K_o = 1.4$ MPa $\sqrt{m}$ for YM-Si_3N_4; the former is plotted on Fig. 2 along with the measured fatigue threshold data. These are also shown in Fig. 1 (as $K_o(1 - R)$) as a lower bound to the predicted threshold for the onset of extension of an absolutely unbridged crack.

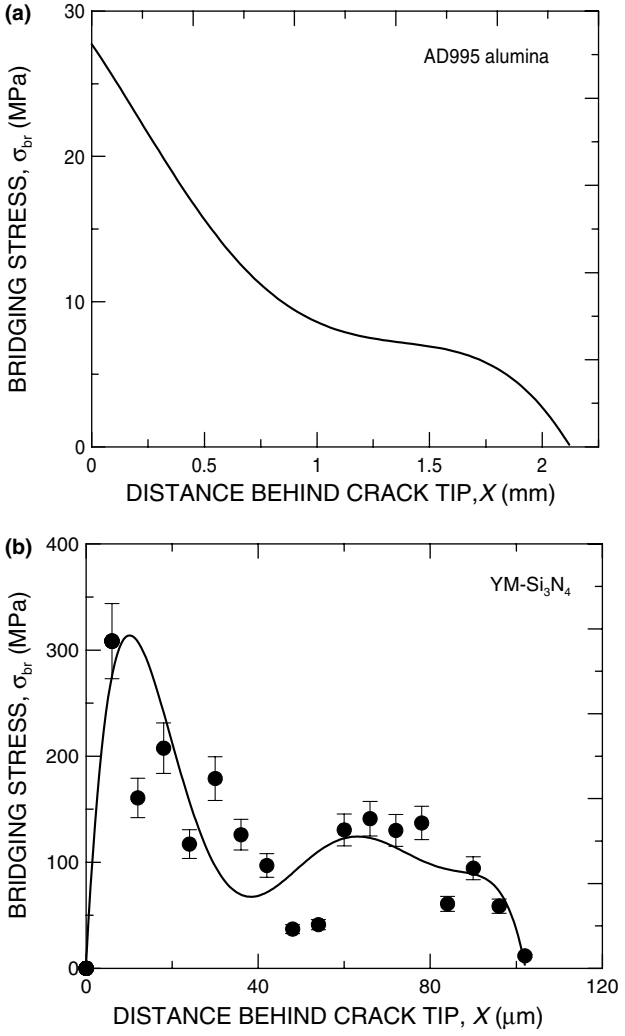

Fig. 3. Deduced bridging stress distributions for (a) AD995 alumina and (b) YM-Si_3N_4. In (b), each data point corresponds to an individual measurement using Raman spectroscopy methods, while the line is a 6th order best-fit polynomial function.

Eqs. (7), (8) may be applied to make predictions of the fatigue threshold *R*-curves based on the bridging stress distributions in Fig. 3, as shown in Fig. 4. A fraction of the additional 0.1 MPa $\sqrt{m}$, that must be included in K_{br} to get an accurate assessment, is added in linear proportion to the crack extension, such that when $\Delta a_f = L$, the full 0.1 MPa $\sqrt{m}$ is added to provide the steady-state value, $K_{SS,br}$ These predicted fatigue threshold *R*-curves, shown in Fig. 4, are in terms of K_{max}, In Fig. 4(a), the actual fatigue threshold data for AD995 alumina are also shown for comparison. While threshold data are currently unavailable for short crack sizes in YM-Si_3N_4, the plateau of the *R*-curve in Fig. 4(b) corresponds to the long-crack fatigue threshold data from Fig. 1(b).

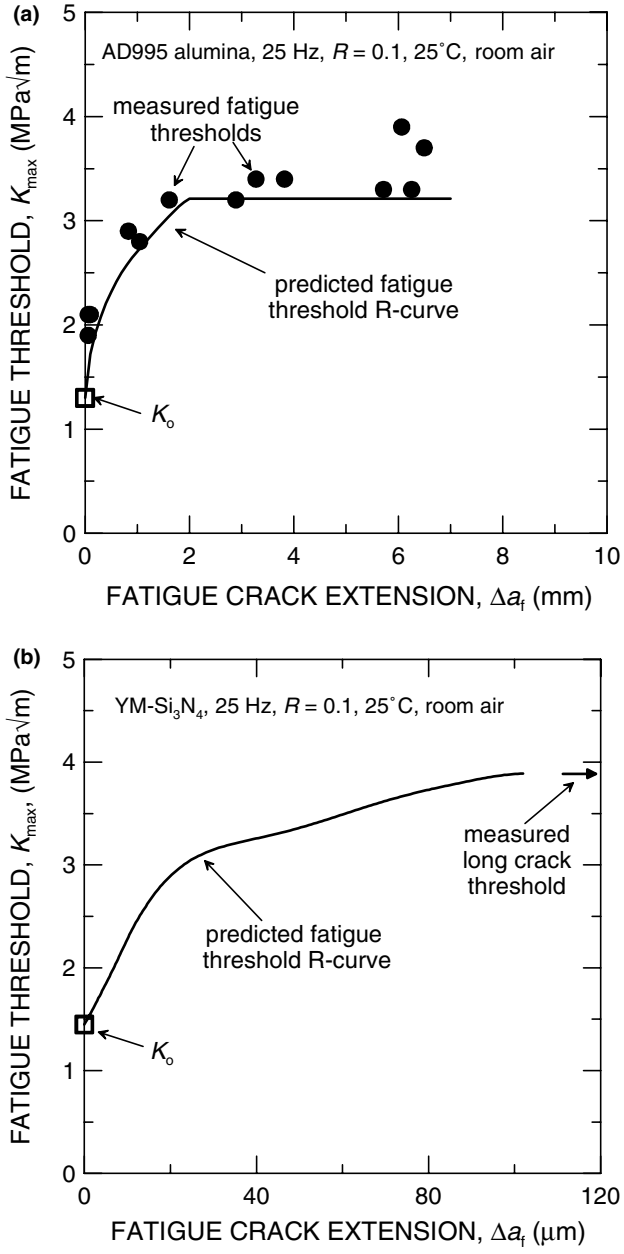

Fig. 4. Predicted fatigue threshold *R*-curves for (a) AD995 alumina and (b) YM-Si_3N_4. Note in (a) that all of the actual measured fatigue thresholds lie on or above the estimate predicted using Eqs. (7), (8) and in (b) the measured long crack threshold lies at the predicted line for $\Delta a_f > 102$ μm.

5. Discussion

It is apparent in Fig. 4(a) that the predicted fatigue threshold *R*-curve provides a conservative estimate of the real thresholds below which cracks were not observed to propagate over the full range of transient crack sizes up to the steady-state regime. The conservative nature of these estimates may lead to discernible differences in deduced parameters, e.g., K_o, compared to results of studies seeking to assess the likely values of these [11,56]. Furthermore, such predictions were made using bridging stress results for long, steady-state fatigue cracks without the need for direct short-crack experiments. This is desirable since direct short/small crack testing over relevant size scales is often prohibitively difficult for many structural ceramics of interest, particularly self-reinforced Si_3N_4 and SiC. To apply the method invoked here successfully, it is imperative, however, to get accurate estimates of the bridging stress distribution for near-threshold fatigue cracks. Two separate methods have been used in present work, involving (i) compliance change and crack-opening profiles from long-crack fatigue-crack growth experiments and (ii) Raman spectroscopy, the latter method being applicable even for small (~100 μm) bridging zones, as in the YM-Si_3N_4.

Inspection of Fig. 1 makes clear that the thresholds for the growth of long fatigue cracks far exceed those for initial extension of an unbridged crack, rendering each of these quantities unsuitable as simple design limits. It is notable that for some short cracks, the velocities initially decay and then accelerate, whereas for others the rates effectively decay to zero. Whether one type of behavior or the other occurs depends on the loading conditions and the evolution of the bridging induced increase in fracture resistance. The use of the threshold *R*-curve allows an explicit description of this, which is elucidated in the next section for cracks in infinite bodies under constant stress conditions.

5.1. Reliability predictions

By expressing the fatigue threshold in terms of K_{max} as seen in Figs. 2 and 4, the fatigue threshold *R*-curve can be plotted along with the fracture toughness *R*-curve, outlining regimes of crack stability behavior for both cyclic and monotonic loading conditions. Fig. 5(a) shows both the predicted fatigue threshold *R*-curve from Fig. 4(a) plotted along with the fracture toughness *R*-curve for the same alumina taken from Refs. [11,56]. Thus, *R*-curve results for both fatigue and fracture behavior can be expressed on one simple plot. The complete fracture toughness *R*-curve is not available for the YM-Si_3N_4, but recent studies have shown that the toughness rises quickly to a plateau level of 7.0 MPa $\sqrt{m}$ in <200 μm of crack growth [43,57]. Thus, to illustrate the comparative behavior for this material, a provisional but conservative *R*-curve was constructed by assuming that it rises to the reported plateau level at least as fast as the fatigue threshold *R*-curve initially rises, shown in Fig. 5(b). For comparison, it has recently been shown that the toughness of a dense Si_3N_4 material that exhibits transgranular fracture is ~ 2.3 MPa $\sqrt{m}$ [57].

Based on the two *R*-curves, for monotonic loading and the cyclic loading threshold, several curves are

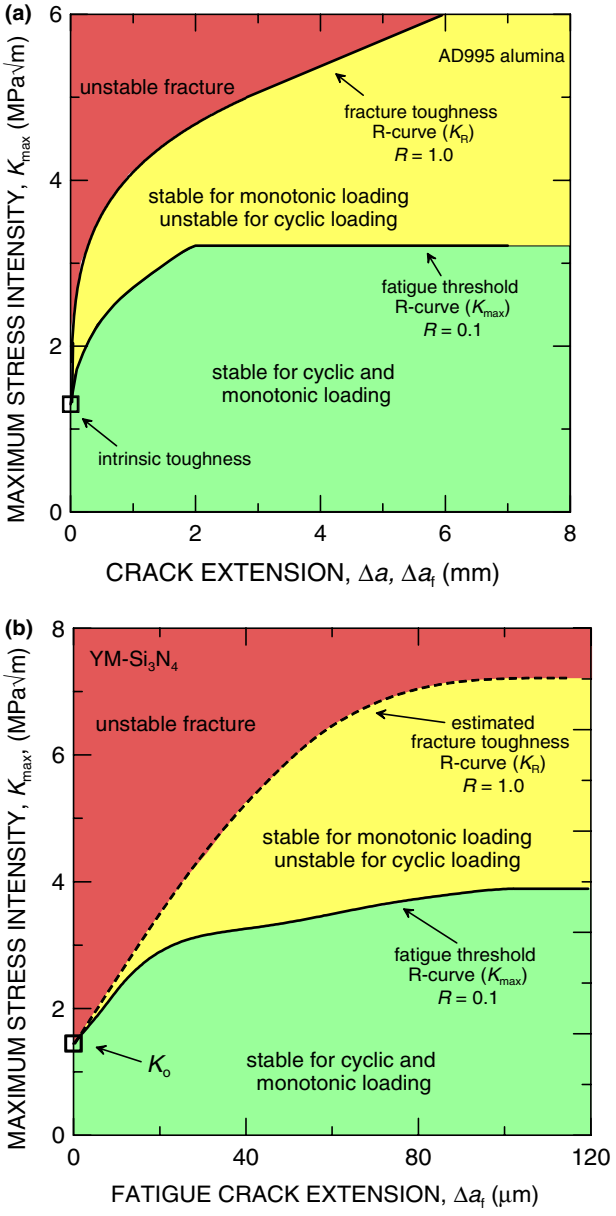

Fig. 5. Plot of the fatigue threshold R-curve and fracture toughness R-curve for (a) AD995 alumina and (b) YM-Si_3N_4, illustrating regimes of stable behavior for both monotonic and cyclic loading conditions.

plotted (Fig. 6) for strength versus initial flaw size, a_i computed using:

$$\sigma = \frac{K_R}{\sqrt{\pi a}}, \tag{9a}$$

$$\frac{dK_{app}}{da} = \frac{dK_R}{da}. \tag{9b}$$

Here and in Fig. 6, the flaw size, a, refers to the full length of a surface flaw, or half-length of a subsurface flaw; the initial flaw is taken to be free of bridging. Fig. 6 demonstrates the utility of the fatigue threshold R-curves by plotting the predicted maximum cyclic

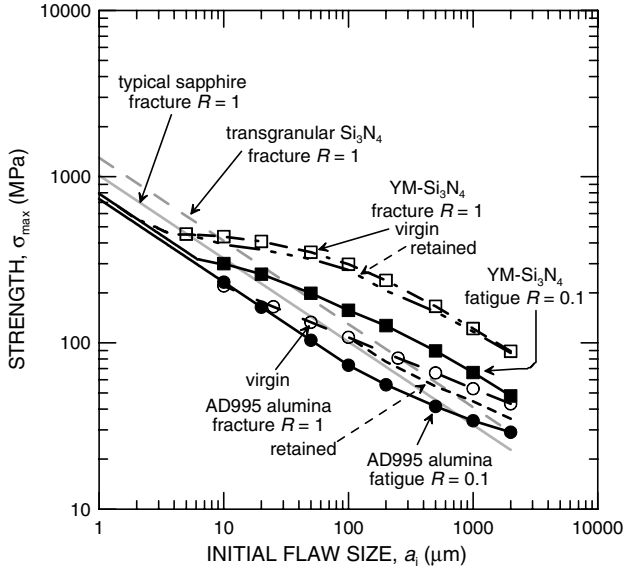

Fig. 6. Predicted endurance strengths as a function of initial flaw size for AD995 alumina and YM-Si_3N_4 based on the fatigue threshold R-curves in Fig. 4. For comparison, the predicted overload failure strengths for AD995 Al_2O_3, based on measured R-curve data from Fig. 5 [11], and for sapphire are also shown both for virgin material and for the as-retained strength for flaws grown to arrest under cyclic loading. Similar strengths are shown for the YM-Si_3N_4, based on the estimated R-curve from Fig. 5 and for a Si_3N_4 that experiences transgranular fracture. Finally, retained overload strengths are predicted for both AD995 alumina and YM-Si_3N_4, representative of samples that were fatigue cycled at the endurance strength and which experienced some crack extension prior to arrest, giving lower strength than virgin material.

stress, σ_{max}, just sufficient to cause fatigue failure, essentially the fatigue endurance strength for $R = 0.1$, versus the initial flaw size, a_i. The endurance strength was calculated analogously to the way monotonic strength is predicted from fracture toughness R-curves:

$$\sigma_{max} = \frac{K^{TH}_{max}}{\sqrt{\pi a}}, \tag{9c}$$

$$\left.\frac{dK_{max}}{da}\right|_{app} = \frac{dK^{TH}_{max}}{da}, \tag{9d}$$

as shown schematically in Fig. 7. Using such relationships, predictions of reliability relevant to cyclic loading conditions can be readily determined in the form of the endurance strength as a function of flaw size and compared with strengths for monotonic loading; this is shown in Fig. 6. For maximum applied (cyclic) stresses below this level, cracks would either not propagate, or arrest after some amount of crack extension, while for stresses above this predicted endurance strength, the structure should fail after some amount of cycling. Due to the high Paris exponents in ceramics, the number of cycles to failure would be expected to be small, which provides the motivation for reliability predictions based on fatigue thresholds. For comparison two values of

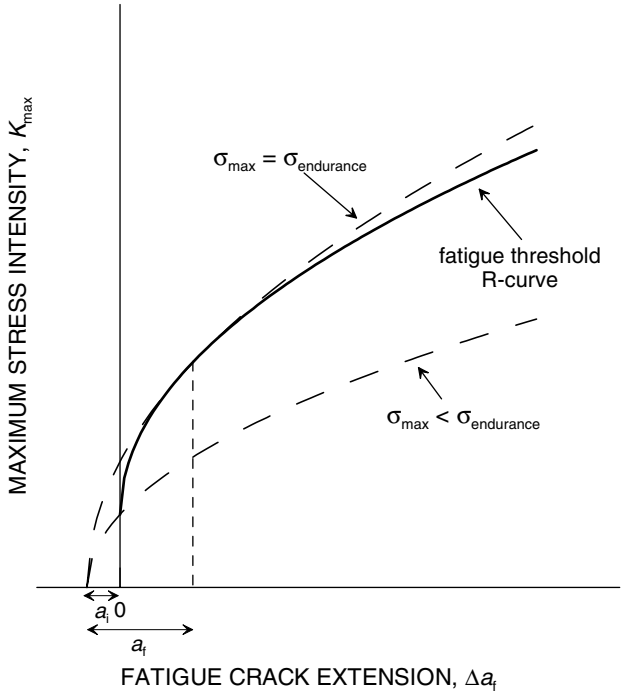

Fig. 7. Schematic illustrating how the fatigue endurance strength may be found using the fatigue threshold *R*-curve for a flaw with initial length, a_i. Additionally, the final crack length after crack arrest, a_f, may be determined, which may be used to subsequently estimate the retained fracture strength using the fracture toughness *R*-curve.

strength under monotonic loading are shown: one for virgin material and the second for the case in which an initial flaw has first grown under cyclic loading until arrest at the fatigue threshold condition, termed the retained strength. For the latter, the starting crack size for the monotonic reloading is conservatively taken as the initial flaw size plus the increment of crack extension under cyclic loading at the endurance strength (i.e., a_f in Fig. 7), but for both parts all bridging is discounted.

Also shown in Fig. 6 are the expected properties for sapphire based on data from Refs. [58–61], and for transgranular Si_3N_4 [57]. The strengths of both single crystal and polycrystalline Al_2O_3 are reduced by testing in moist environments, which even influences the *R*-curves, as shown recently in Ref. [56]. To make comparisons more meaningful, strengths for sapphire were computed using a toughness of $0.75K_c$; this is used as slow crack growth curves show that the subcritical crack-growth thresholds occur at about $0.5K_c$, where K_c is for fracture in inert conditions or at higher velocity [59,62–64], and the present testing is at intermediate velocities.

Note that although both AD995 alumina and YM-Si_3N_4 have similar intrinsic fatigue thresholds, $K^{TH}_{o,max}$, and long crack toughnesses, the Si_3N_4-based ceramic has much higher predicted monotonic strengths and endurance limits at relevant flaw sizes due to the more steeply rising *R*-curves. This demonstrates how simply using the intrinsic fatigue threshold as a design parameter would be overly conservative since subcritically growing cracks will often arrest in materials with rising fatigue threshold *R*-curves. It is also evident from these curves that a material with the rapidly rising and robust *R*-curve can provide significant advantage over the untoughened material in both monotonic and fatigue situations. In contrast, for this Al_2O_3 material, the benefits of toughening are virtually eliminated for any flaw sizes of interest by comparison with the behavior of sapphire under cyclic loading. To reinforce these comparisons it is noted that the unreinforced materials are not expected to exhibit crack growth induced by cyclic fatigue, so that the curves shown as virgin strength essentially also denote the endurance and retained strengths.

5.2. Effects of load ratio

When considering the expected effect of load ratio on the fatigue threshold *R*-curves seen in Fig. 4, it is noted that the fracture toughness *R*-curve, which experiences no cyclic loading, is essentially determined at a load ratio of $R = 1$, i.e., the minimum and maximum loads are equal (Fig. 5). It is be expected then that the $R = 0.1$ fatigue threshold *R*-curve should be conservative for load ratios higher than 0.1 since the fatigue behavior should approach monotonic fracture as the load ratio is increased. This is because as the load ratio is increased, the value of ΔK, which determines the amount of bridging degradation, falls for a given value of K^{TH}_{max} [41]. Indeed, this notion is supported by fatigue data for bridging ceramics which show an increase in the K^{TH}_{max} fatigue threshold with increasing load ratio over a range of R from 0.1 to 0.9 [14,65,66]. Thus, for positive load ratios less than one (i.e., tension–tension loading), it is expected that measurements at the minimum expected service load ratio would result in a conservative fatigue threshold *R*-curve for making predictions of reliability.

It then follows that predictions for positive load ratios may be non-conservative for reversed loading (i.e., negative load ratios) since at a given K_{max} value, ΔK would be higher and the amount of bridge degradation would be expected to be more severe. Unfortunately, experimental data for $R < 0$ is limited (e.g., Refs. [67,68]) and direct comparisons to data for $0 < R < 1$ are unavailable. However, this notion would be in agreement with compression-compression fatigue results where R values exceed one; here, the fatigue resistance is lower at higher load ratios (ranging from 2 to 8) [69], suggesting that compressive cycling is progressively more damaging with increasing load ratio.

5.3. Final comments

Only one sample of the Si_3N_4 was used in the present work and served to demonstrate the applicability of the

proposed methods. To obtain a conservative fatigue threshold *R*-curve for design purposes, however, more experiments would be needed to account for scatter in the fatigue threshold, as seen for AD995 alumina in Figs. 1(a) and 2. Moreover, as with AD995 alumina, care must be taken to determine the predicted fatigue threshold *R*-curve using conservative values.

The methods presented here are strictly only applicable to functionally-short/small cracks, and the integral in Eq. (7) should be redone to reflect the pertinent geometry. Where crack sizes approach the scale of characteristic microstructural features, additional effects due to limited sampling of the microstructure and residual stresses may play more dominant roles. Lawn and coworkers [35–37] have recognized and modeled the effects of the additional driving forces due to residual stresses, e.g., from thermal expansion mismatch. Tensile stresses that act around a grain under residual compression aid initial extension of a small adjacent flaw, with this effect decaying as the crack grows out of the residual field. If unaccounted, this can reduce the effective *R*-curve for extension over dimensions of the order of the size of the stressed grain, even to the extent of allowing some spontaneous fracture. However, as the crack grows beyond this residual field, the effective *R*-curve can rise very rapidly and may quickly approach that for a short crack. In that instance, the effect is to cause a limiting strength at small flaw sizes rather than the usual continued rise in the strength-flaw size curve. Such effects could be added analytically in combination with the experimentally-derived, short-crack *R*-curves. Also chemical or microstructural heterogeneities may reduce early parts of an *R*-curve and similarly limit the achievable strength at small sizes.

Finally, the principles described here may be extended to other bridging materials and should not be limited to ceramics. For brittle and semi-brittle materials such as bridging intermetallic compounds and brittle metal alloys (e.g., below the ductile-brittle transition temperature) which have similarly high Paris exponents (e.g., see Refs. [70,71]), the fatigue threshold should also be the most relevant design parameter for cyclic loading conditions, and a similar methodology could easily be adopted provided accurate bridging stress profiles can be determined. Furthermore, some high-cycle fatigue situations, e.g., blades in gas-turbine engines, involve very high cycling frequencies such that even relatively ductile metals such as titanium- and nickel-base alloys will fail quickly if the fatigue threshold is exceeded, providing limited useful service life. For materials used in these high-cycle fatigue applications that experience crack bridging, methods similar to those described here could be applied. It is important to note, however, that as materials become more ductile there will be an increasing role of crack closure in affecting the fatigue threshold which must be considered as well.

6. Conclusions

Based on an experimental study of fatigue-crack growth thresholds in grain-bridging ceramics (Al_2O_3 and Si_3N_4), the following conclusions are made:

1. The effect of crack size on the threshold for fatigue-crack growth may be expressed in terms of a fatigue threshold *R*-curve, which is analogous to the classical fracture toughness *R*-curve and may be used for predictions of the endurance strength under cyclic loading conditions.
2. Using measured bridging stress profiles, the fatigue threshold *R*-curve for short cracks may be predicted based solely on results from many millimeter long, through-thickness, fatigue cracks. Direct comparisons of predictions to experimentally measured fatigue-crack growth thresholds in AD995 Al_2O_3 over a range of crack sizes demonstrate the accuracy of such methods.
3. The methods presented here offer a basis for an alternative to difficult and costly short/small crack fatigue experiments needed to determine the fatigue behavior, i.e., the threshold for crack growth and the retained strength after fatigue crack arrest, at relevant crack sizes for ceramic materials. However, work remains to assess modifications proposed for application to microstructurally-small cracks.
4. These methods provide a tangible means to assess the expected degradation of toughening mechanisms for cracks in ceramics subjected to cyclic loading. Although the cracking resistance is invariably degraded by cyclic loading, in some instances such degradation offsets any benefits of toughening for flaw sizes of any interest; whereas, in situations with sufficiently rapidly rising and resilient *R*-curves, then even with the degraded bridging, short cracks will arrest after a small amount of growth, leaving significant useful residual strength. Such behavior can be quantitatively described based on relatively accessible measurements of either threshold *R*-curves directly or bridging functions from long, near-threshold fatigue cracks, and these methods may be extended to bridging materials other than ceramics as well.

Acknowledgments

This work was supported by the Director, Office of Science, Office of Basic Energy Sciences, Division of Materials Sciences and Engineering of the US Department of Energy under Contract No. DE-AC03-76SF00098. The authors gratefully acknowledge Drs. M.J. Hoffmann and R.L. Satet (University of Kar-

lsruhe) for providing the Si_3N_4 material and Ms. K.L. Breeden for aid in analyzing the Raman spectra.

References

[1] Swanson PL, Fairbanks CJ, Lawn BR, Mai Y-W, Hockey BJ. J Am Ceram Soc 1987;70:279.
[2] Mai Y-W, Lawn BR. J Am Ceram Soc 1987;70:289.
[3] Vekinis G, Ashby MF, Beaumont PRW. Acta Metall Mater 1990;38:1151.
[4] Gilbert CJ, Cao JJ, De Jonghe LC, Ritchie RO. J Am Ceram Soc 1997;80:2253.
[5] Li C-W, Lee D-J, Lui S-C. J Am Ceram Soc 1992;75:1777.
[6] Hay JC, White KW. J Am Ceram Soc 1993;76:1849.
[7] Padture NP. J Am Ceram Soc 1994;77:519.
[8] Padture NP, Lawn BR. J Am Ceram Soc 1994;77:2518.
[9] Gilbert CJ, Cao JJ, MoberlyChan WJ, De Jonghe LC, Ritchie RO. Acta Metall Mater 1996;44:3199.
[10] Lathabai S, Rödel J, Lawn B. J Am Ceram Soc 1991;74:1348.
[11] Kruzic JJ, Cannon RM, Ritchie RO. J Am Ceram Soc 2004;87:93.
[12] Gilbert CJ, Dauskardt RH, Ritchie RO. J Am Ceram Soc 1995;78:2291.
[13] Gilbert CJ, Petrany RN, Ritchie RO, Dauskardt RH, Steinbrech RW. J Mater Sci 1995;30:643.
[14] Gilbert CJ, Ritchie RO. Fatigue Fract Eng Mater Struct 1997;20:1453.
[15] Okazaki M, McEvily AJ, Tanaka T. Metall Trans 1991;22A:1425.
[16] Guiu F, Li M, Reece MJ. J Am Ceram Soc 1992;75:2976.
[17] Dauskardt RH. Acta Metall Mater 1993;41:2765.
[18] Dauskardt RH, Ritchie RO. Closed Loop 1991;17:7.
[19] Anderson TL. Fracture mechanics fundamentals and applications. 2nd ed. CRC Press; 1995. p. 688.
[20] Fett T, Munz D, Dai X, White KW. Int J Fract 2000;104:375.
[21] Lawn B. Fracture of brittle solids. Cambridge University Press; 1993. p. 378.
[22] Fett T, Munz D, Seidel J, Stech M, Rödel J. J Am Ceram Soc 1996;79:1189.
[23] Pippan R, Berger M, Stüwe HP. Metall Trans 1987;18A:429.
[24] Tanaka K, Akiniwa Y. Eng Fract Mech 1988;30:863.
[25] Tabernig B, Pippan R. Eng Fract Mech 2002;69:899.
[26] Chen I-W, Liu S-Y. J Am Ceram Soc 1991;74:1197.
[27] Dauskardt RH, James MR, Porter JR, Ritchie RO. J Am Ceram Soc 1992;75:759.
[28] Ritchie RO. Int J Fract 1999;100:55.
[29] Chen D, Shirato K, Barsoum MW, El-Raghy T, Ritchie RO. J Am Ceram Soc 2001;84:2914.
[30] Huh Y-H, Song J-H. Fatigue Fract Eng Mater Struct 1998;21:1575.
[31] Chen D, Gilbert CJ, Zhang XF, Ritchie RO. Acta Mater 2000;48:659.
[32] Ritchie RO, Lankford J. Mater Sci Eng A 1986;84:11.
[33] Suresh S, Ritchie RO. Int Metals Rev 1984;29:445.
[34] Ritchie RO, Yu W. In: Ritchie RO, Lankford J, editors. Small fatigue cracks. Warrendale, PA: TMS-AIME; 1986. p. 167.
[35] Bennison SJ, Lawn BR. Acta Metall 1989;37:2659.
[36] Chantikul P, Bennison SJ, Lawn BR. J Am Ceram Soc 1990;73:2419.
[37] Lathabai S, Lawn BR. J Mater Sci 1989;24:4298.
[38] Mutoh Y, Miyashita Y, Zhu S. In: Ravichandran KS, Ritchie RO, Murakami Y, editors. Small fatigue cracks: mechanics, mechanisms, and applications. Oxford, UK: Elsevier; 1999. p. 259.
[39] Gilbert CJ, Han YS, Kim DK, Ritchie RO. Ceram Int 2000;26:721.
[40] Han YS, Kim DK, Gilbert CJ, Ritchie RO. J Am Ceram Soc 2001;84:551.
[41] Chen I-W, Engineer M. J Am Ceram Soc 1999;82:3549.
[42] Satet RL, Hoffmann MJ. J Euro Ceram Soc 2004;24:3437.
[43] Satet RL, Hoffmann MJ. J Am Ceram Soc 2005 [in press].
[44] Satet RL. Ph.D., University of Karlsruhe, Karlsruhe, 2003.
[45] Deans WF, Richards CE. J Test Eval 1979;7:147.
[46] Dowling NE. Fatigue Eng Mater Struct 1979;2:129.
[47] Palazotto AN, Mercer JG. Eng Fract Mech 1990;37:473.
[48] Wittmann FH, Hu X. Int J Fract 1991;51:3.
[49] Fett T, Munz D. Stress intensity factors and weight functions. Computational Mechanics Publications; 1997. p. 408.
[50] Fett T, Mattheck C, Munz D. Eng Fract Mech 1987;27:697.
[51] Sergo V, Pezzotti G, Katagiri G, Muraki N, Nishida T. J Am Ceram Soc 1996;79:781.
[52] Pezzotti G. J Raman Spectrosc 1999;30:867.
[53] Pezzotti G, Muraki N, Maeda N, Satou K, Nishida T. J Am Ceram Soc 1999;82:1249.
[54] Pezzotti G, Ichimaru H, Ferroni LP, Hirao K, Sbaizero O. J Am Ceram Soc 2001;84:1785.
[55] Bueckner HF. Z Angew Math Mech 1970;50:529.
[56] Kruzic JJ, Cannon RM, Ritchie RO. J Am Ceram Soc 2005 [in press].
[57] Satet RL, Kruzic JJ, Hoffmann MJ, Cannon RM, Ritchie RO. J Am Ceram Soc 2005 [to be submitted].
[58] Wiederhorn SM. J Am Ceram Soc 1969;52:485.
[59] Wiederhorn SM, Hockey BJ, Roberts DE. Philos Mag 1973;28:783.
[60] Becher PF. J Am Ceram Soc 1976;59:59.
[61] Iwasa M, Bradt RC. Structure and properties of MgO and Al_2O_3 ceramics. In: Kingery WD, editor. American Ceramic Society, Columbus, OH; 1984. p. 767.
[62] Evans AG. J Mater Sci 1972;7:1137.
[63] Wiederhorn SM. Int J Fract Mech 1968;4:171.
[64] De Aza AH, Chevalier J, Fantozzi G, Schehl M, Torrecillas R. Biomaterials 2002;23:937.
[65] Zhan G-D, Reece MJ, Li M, Calderon-Moreno JM. J Mater Sci 1998;33:3867.
[66] Ueno A, Kishimoto H, Kawamoto H, Asakura M. Eng Fract Mech 1991;40:913.
[67] Fett T, Martin G, Munz D, Thun G. J Mater Sci 1991;26:3320.
[68] Reece MJ, Guiu F, Sammur MFR. J Am Ceram Soc 1989;72:348.
[69] Sabadell JM, Anglada M. J Mater Sci Lett 1990;9:964.
[70] Kruzic JJ, Campbell JP, Ritchie RO. Acta Mater 1999;47:801.
[71] Kruzic JJ, Schneibel JH, Ritchie RO. Scripta Mater 2004;50:459.